Check for updates

"Close network" effect of a ZnO micro/nanoporous array allows high UV-irradiated NO₂ sensing performance†

Xingsong Su,[ab] Lei Gao,[a] Fei Zhou,[a] Weiping Cai[a] and Guotao Duan [ID] *[a]

ZnO micro/nanoporous arrays with controlled morphologies were fabricated by a monolayer colloidal crystal and solution-dipping strategy. Then their UV-irradiated NO₂ sensing performances, especially the morpholgy-correlated effects were studied in detail. It was found that a close-network micro/nanoporous array film (CNPAF) and bowl-like micro/nanoporous array film (BLPAF), which were prepared with different concentrations of precursors, presented different sensing performances. The former showed higher sensitivity, lower detecting limit, and shorter response/recovery times. The "close network" effect was proposed to explain the mechanism behind these results. First, CNPAF has a closed network structure, which would decrease the resistance of the film and provide more sensing spots for NO₂, which enhanced sensitivity. Second, according to the hydrokinetics of microluidic flow, the closed network structure may localize the flowing gas, which led to shorter response and recovery times of the sensor. This work clarified the morphology-correlated effect of ZnO micro/nanoporous arrays on their NO₂ sensing performances, and it would be helpful for the realization of room temperature NO₂ sensors.

Introduction

Nitrogen dioxide (NO₂) is a combustion-supporting material and main atmospheric pollutant that causes acid rain and even explosion.[1,2] So it is urgently needed to detect or monitor ppb-level NO₂ in the field of detecting explosions with high performance NO₂ sensors.[3,4] Semiconductor gas sensors are becoming more and more attractive in NO₂ detection in recent years because of their high sensitivity, long-term stability and quicker response and recovery times.[5–8] However, for the traditional semiconductor gas sensors, they are generally operated at a high temperature (175–400 °C).[9,10] The high operation temperature limits the applications of gas sensors in many areas. Such high operating temperatures may induce ignition of flammable and explosive gases, and also cause high power consumption of the sensors.

To solve the above problems, a few room temperature NO₂ sensors have been designed and manufactured by using new sensitive materials[11,12] and new techniques, such a micro-electro mechanical system (MEMS) fabrication,[13] doping of novel metals[14,15] and ultraviolet (UV) irradiation *etc.*[16,17] In these techniques, UV irradiation has attracted increasing attention as

a promising strategy. It has been reported that a large number of photo-generated carriers diffuse to the surface of semiconductor under UV irradiation. Then the charge carries are involved in the reaction with electron donors or acceptors readily, which induces the change of photocurrent intensity.[18–20] Based on the above theory, many researchers have found that UV irradiation can improve the sensing performance of semiconducting gas sensors.

Zinc oxide (ZnO), with a wide band gap of 3.37 eV, has been considered as one of the promising materials in the field of gas sensors operated under UV light irradiation.[21–24] The sensing performances and optical properties of ZnO based devices are influenced significantly by its surface morphologies. So many researches were focused on the formation of various morphology of ZnO thin film with one step physical deposition routes, such as vacuum evaporation and sputtering methods.[25–28] Alternatively, ZnO film can also be deposited by spin- or dip-coating method using ZnO slurry.[29–31] However, these techniques usually show some drawbacks. For instance, the one step physical deposition routes usually have the acknowledged disadvantages of high cost, while ZnO thin films obtained by the spin- or dip-coating techniques are mostly limited to flat substrates, difficult to maintain uniform on a large scale. The presence of irregular interstitial areas and inhomogeneous aggregations leads to poor repeatability and uncertain performance of the finally ZnO devices. In recent years, colloidal lithography by using polystyrene sphere (PS) monolayer colloidal crystal (MCC) have been proven an effective method to synthesize micro/nanostructured arrays film with

[a]Key Lab of Materials Physics, Anhui Key Lab of Nanomaterials and Nanotechnology, Institute of Solid State Physics, Chinese Academy of Sciences, Hefei, 230031, PR China. E-mail: duangt@issp.ac.cn

[b]University of Science and Technology of China, Hefei, 230026, PR China

nice homogeneity. Thus it can also be used as strategy to formation gas-sensing film sensors.[32–34]

In this work, ZnO micro/nanostructured arrays films of different morphologies were fabricated based on PS MCC, and their sensing properties under UV irradiation were also studied. It has been found that the sensing performances are strongly morphology-dependence: ZnO CNPAF sensors show higher sensitivity, lower detecting limit and shorter response/recovery time compared to ZnO BLPAF sensor. Then a "close network" effect is further proposed to explain the behind mechanism. This work clarified the morphology-correlated effect of ZnO micro/nanoporous arrays on their NO$_2$ sensing performances, which is very important for the realization of NO$_2$ room temperature sensors. The results and discussion are detailed in the following sections.

Experimental section

Fabrication of ZnO micro/nanoporous porous films

The fabrication of PS (500 nm) monolayer colloidal crystal (PS MCC) follows our previous report with a minor modification.[35–38] The freshly fabricated PS MCC on the glass slides possesses the feature of transferability. The transfer process from the glass slide to a silicon wafer (20 mm × 20 mm), glass slide (50 mm) or a flat ceramic electrode (2.5 mm × 2.0 mm) substrate is illustrated in Fig. 1c, d and S1 (see ESI†). The transferred PS MCC on the flat substrate was firstly surface-modified by irradiation in the ultraviolet ozone cleaner for 5 min to improve its mechanical flexibility and surface hydrophilicity. Then 0.1 mol L^{-1} and 0.2 mol L^{-1} Zn(AC)$_2$·2H$_2$O were taken as precursor solutions. When immersed into the precursor solution, the PS MCC template was separated from the glass slide and integrally floated on the surface of the precursor, as shown in Fig. 1c. Then, a flat substrate was used to pick up the template carefully, as shown in

Fig. 1d. The samples were dried at 80 °C for an hours. The final annealing was carried out at 450 °C for 2 h to remove the PSs in air, leaving a bowl-like or close-network micro/nanoporous porous films on the substrate, forming ZnO due to the decomposition of Zn(AC)$_2$·2H$_2$O. The heating rate and cooling rate were about 2 °C min^{-1}.

Characterization and gas sensing measurements

The microstructures and morphologies of the as-prepared samples were characterized by using field-emission scanning electron microscopy (FEEM, Srion200). Phase formation of the films were carried out on a Philips X'pert powder X-ray diffractometer using Cu$_{K\alpha}$ radiation (0.15419 nm). Gas sensing properties were measured for the ZnO porous films covered on Al$_2$O$_3$ flat ceramic substrate using a static test system which includes a test chamber and a multimeter/DC power supply (Agilent mod. U3606A and U8002A). The photoelectric gas sensing measurement was carried out under irradiation of monochromatic light (365 nm) (CEL-LED 100-365, Aulight). The UV light was adjusted to 5 W and the distance between the UV lamp and the thin film sample was 15 cm. The light beam was 8 cm in diameter and vertically irradiated on the sensing film through a quartz window on the test chamber. The UV light was turned on after the film was put into the test chamber. After a steady resistance was measured for the film, a certain amount of NO$_2$ was injected into the test chamber and the response was measured. The NO$_2$ concentration in the chamber was calculated according to the injected amount. After the irradiation for ~1000 s, the UV light was turned off. All measurements were operated at room temperature (25 °C).

Results and discussion

The samples were fabricated by taking transferred PS monolayer colloidal crystal (MCC) template and sequent heat
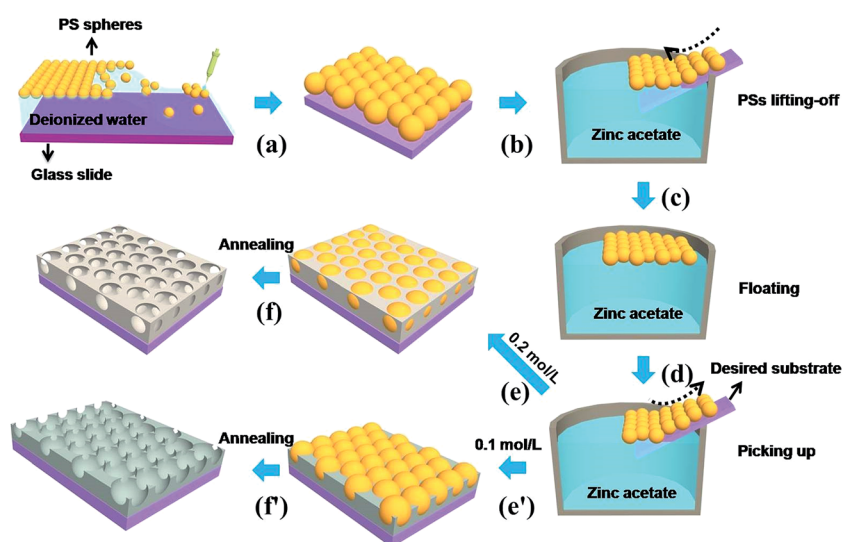

Fig. 1 Schematic illustration of fabrication routes: the processing steps used to *in situ* fabricate ZnO ordered porous an Al$_2$O$_3$ flat ceramic electrodes. (b) The colloidal template is stripped off and (c) floated on the surface of precursor solution; (d) the floating monolayer colloidal template is picked up by the Al$_2$O$_3$ flat ceramic electrodes; (e) and (e′) the Al$_2$O$_3$ flat ceramic electrodes covered with monolayer colloidal template is dried in the dying oven; (f) and (f′) the ZnO micro/nanoporous array-film is formed after annealing at a high temperature (450 °C).
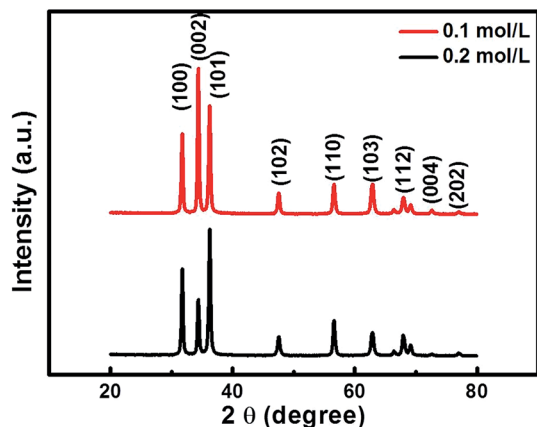
Fig. 2 XRD pattern of ZnO micro/nanoporous ordered arrays: (a) 0.1 mol L^{-1}; (b) 0.2 mol L^{-1}.

treatment, as is shown in Fig. 1. Fig. 2 shows the XRD pattern of the as-prepared samples. All diffraction peaks can be indexed to a wurtzite structure of the ZnO material (JCPDF card no. 00-036-1451), no characteristic peaks from other crystalline forms are detected in the XRD pattern.

Fig. 3 shows the SEM images of ZnO micro/nanoporous ordered arrays (on a silicon wafer substrate), with different precursor concentrations, dried in an oven at 80 °C for an hours, and then heated at 450 °C for two hours. A series of porous ordered arrays with different morphologies was obtained. When the precursor concentration is 0.1 M or 0.2 M, the micro/nanoporous array films with uniform pore size was formed on the flat substrates, as shown in Fig. 3A and C. The micro/nanoporous array films with two different morphologies were more clearly revealed by tilted views, as illustrated in Fig. 3B and D. A low concentration (0.1 M) gives rise to pores with nearly circular upper-end openings, which is called bowl-like structure (Fig. 3B). As the precursor concentration increases to 0.2 M, it is found that some small holes at the interstitial position of the closely packed PSs and nanogaps on pore walls (skeletons) appear. The micro/nanoporous arrays film is actually a nearly

Fig. 3 SEM images of ZnO micro/nanoporous arrays obtained from 500 nm PS film templates at different precursor content of zinc acetate (Zn(AC)$_2$·2H$_2$O): (A and B): 0.1 mol L^{-1}; (C and D): 0.2 mol L^{-1}. (B) and (D) are oblique views.

spherical hollow array with truncated tops as openings, which is named as close-network structure (Fig. 3D). The thickness of the CNPAF and BLPAF are 400 nm and 280 nm, respectively (Fig. S2†). The truncated hollow sphere arrays with these close networks structure are a key factor to enhance sensing performances compared to the micro/nanoporous arrays film of bowl-like. We can also fabricate a larger area of micro/nanostructure porous ordered array film (Fig. S3 see ESI†).

The gas sensing properties of the ZnO micro/nanoporous arrays films for NO$_2$ were measured under UV light irradiation at room temperature. The gas response of sensors is defined as (R_{gas}/R_{air}), where R_{air} is the resistance in air and R_{gas} is the resistance in the presence of NO$_2$ under UV light irradiation (0.35 mW cm^{-2}). The sensitivity increased instantaneously to a maximum sensitivity, which was maintained at the maximum sensitivity upon exposure to NO$_2$ and recovered completely to the initial value upon the removal of NO$_2$. The gas response curves of sensors to different concentrations for NO$_2$ are shown in Fig. 4. It can be seen that the gas response transients exhibited stable and reproducible response and recovery characteristics, and the response increase obviously for two samples with the increasing NO$_2$ concentrations. Fig. 5A presents the response of BLPAFs and CNPAFs as a function of the NO$_2$ concentration. It is obvious that the sensor of CNPAFs exhibits a stronger response to NO$_2$ measured at room temperature under UV light irradiation than the sensor based on BLPAF. For example, the responses of bowl-like ZnO micro/nanoporous array sensor and close-network ZnO micro/nanoporous array sensor to 50 ppm of NO$_2$ were 4.5 and 27.5, respectively. The CNPAF based sensor also exhibited a faster response (Fig. 5B) and recovery time (Fig. 5C) than BLPAF sensor at the same NO$_2$ concentration. For example, the response time of the sensor based on BLPAF to 50 ppm was 125 s, while the response time of the sensor based on CNPAF was 35 s. The recovery time of sensor based on CNPAF to 50 ppm was shortened from 210 s to 65 s corresponding to that of BLPAF based sensor. Herein, the response and recovery times of the sensors are defined as the times to reach 90% of resistance change upon exposure to NO$_2$ and air, respectively. In addition, the gas sensing properties of the CNPAF and BLPAF have good repeatability, as shown in Fig. S4.†

Besides NO$_2$, the sensing performances of the two micro/nanoporous arrays sensors to other gases including H$_2$S, CH$_2$O, C$_2$H$_5$OH, SO$_2$ and CH$_4$ at room temperature were investigated under UV light irradiation, as shown in Fig. 5D. Both the bowl-like and close-network ZnO micro/nanoporous arrays film sensors exhibited a stronger response to NO$_2$ than to other gases. The sensor of CNPAFs showed lower normalized response to the other gases than the BLPAF based sensor, suggesting that the close-network sensor has superior selectivity for NO$_2$ gas compared to the bowl-like sensor. The selectivity of the sensor is influenced by various factors. For the study, the structures and bond dissociation energies of gas molecules are significant influences. The NO$_2$ band is 221 kJ mol^{-1}, which is smaller than other gases at room temperature. Therefore, the bond dissociation energies of NO$_2$ are easily broken to participate in the reaction with the sensing material in the process of
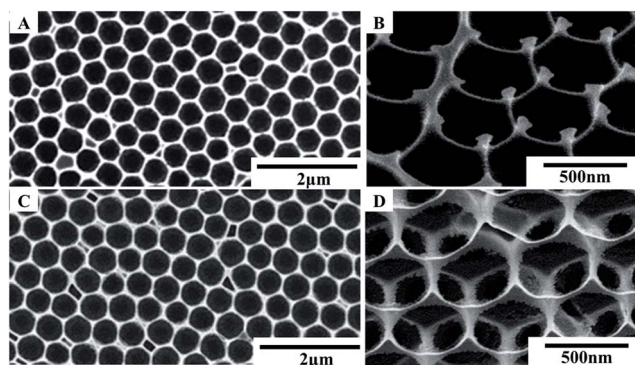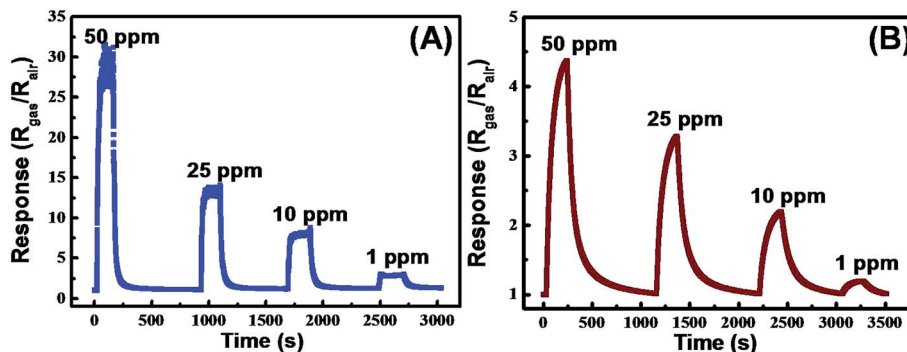
Fig. 4 Gas response transients of close-network ZnO micro/nanoporous array films (A) and bowl-like ZnO micro/nanoporous array films (B) toward NO$_2$ gas at room temperature under UV light irradiation.
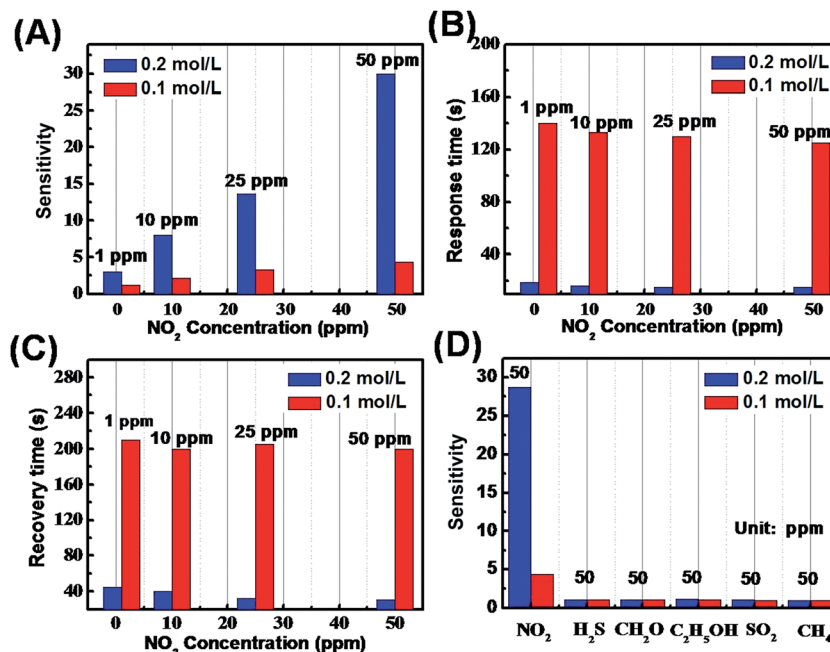

Fig. 5 (A) Response, (B) response time, (C) recovery time of the bowl-like ZnO micro/nanoporous array films and close-network ZnO micro/nanoporous array films toward NO$_2$ gas at room temperature under UV light irradiation. (D) Comparison of response of ZnO micro/nanoporous array gas sensor to different kinds of flammable gases at room temperature under UV light irradiation.

chemical adsorption. In addition, other gases because of their high bonding energy would be reluctant to react at room temperature, but display lower response. So the operating temperature is also an important factor. The operating temperature depends on the orbital energy of gas molecule, adsorption mode and amount of gas and so on[33,34] Therefore, the selectivity may be distinct different operating temperatures. In a word, the high selectivity makes the ZnO micro/nanostructure ordered porous array films to be a remarkable sensing material in fabrication of NO$_2$ sensor.

A low determination limit is important for the gas sensors in trace or ultratrace target gas analysis, especially in practical application. To observe the sensor response to 100 ppb NO$_2$ in ambient gas which even contains low-concentration NO$_2$, the continuous tests without recoveries were taken in the concentration range from 100 ppb to 1000 ppb at room temperature

under UV light irradiation, as shown in Fig. 6. It is obvious that the CNPAF based sensor can determine NO$_2$ gas as low as 100 ppb, while it cannot be detected at such a low concentration by the BLPAF based sensor.

When the sensors are exposed to air at room temperature without UV irradiation, the adsorbed oxygen molecules on the surface of zinc oxide are in a dynamic equilibrium state. The possible model for enhanced sensing performance of the two sensors is shown in Fig. 7. Electrons are transferred from the conduction band to the adsorbed oxygen atoms, and forming ionic species, such as O$^-$, O^{2-} and O$_2^-$ (Fig. 7a and a'). Of these oxygen species, O$_2^-$ is dominant at room temperature.[38–41] When the ZnO films are irradiated with UV light (365 nm) of energy higher than the band gap (3.22 eV), as shown in Fig. S5.† The electrons in the valence band are excited to the conduction band, and holes are generated in valence band. The surface of
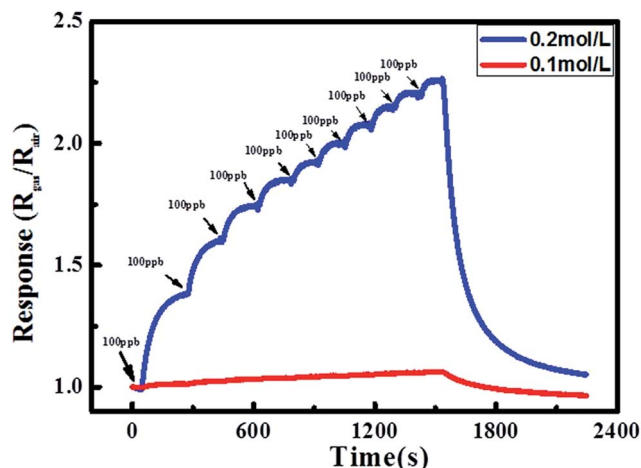
Fig. 6 Continuous test without recoveries to 100–1000 ppb NO_2 concentration range at room temperature under UV light irradiation.

ZnO porous films will generate a large number of photon-generated electrons and holes, and excited electrons move the valence band. On their way to the ZnO micro/nanoporous film surface, some photon-generated electrons and holes will recombine with each other and many photon-generated holes react with negatively charged adsorbed oxygen ions on the surface of ZnO porous films. The result of these reactions is that the width of the surface depletion layer in the skeleton of ZnO porous films is reduced (Fig. 7b and b'). Oxygen species were photodesorbed from the surface.[42] Upon exposure to NO_2 gas, the NO_2 gas adsorbs on the sensors and the remaining photo-generated electrons were released from the material surface, and were attracted to the adsorbed NO_2 molecules because an oxidizing gas, such as NO_2, acts as an electron acceptor (Fig. 7c and c'), as shown in the following reaction:[34,41]

$$2NO_2 \text{ (g)} + e^- \text{ } (hv) \rightarrow 2NO \text{ } (hv) + O_2^- \text{ } (hv)$$
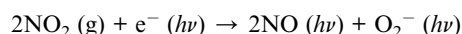
This reaction further broadens the width of the surface depletion layer, which led to increase of the sensors resistance.

To investigate the relationship between crystal morphologies and sensing property, previous publication of the ZnO sensing work have been tabulated, as shown in Table S1.† It is found that the gas properties of sensitive materials with different morphologies are significantly different, such as the response of the needle-like ZnO nanorods is 184.5, while the response of flower-like ZnO nanorods is 44.8. The high response of sensing materials to target gas is due to their high surface-to-volume ratio, which results in more O^- ions adsorption on the material surface. Thus, the possible reaction between the target gas and the O^- ions increased and resulted to the increase of the conduction, which also indicates that the equilibrium density of chemisorbed O^- ions was maximal at the optimum operating temperature. However, the influence of sensitive materials with different morphology to the gas sensing properties are complicated, it not only has to consider the surface-to-volume ratio, but also crystal-lographic orientation of crystalline planes and surface architecture.[43,44] Therefore, the enhanced sensing performance of the CNPAF sensor relative to that of the BLPAF sensor can be explained by a combination of electronic and chemical mechanisms. A critical difference between the CNPAF and BLPAF sensors is the presence of close-network on the top of bowl-like structure sensors, as shown in Fig. 8. It is well know that the gas chemical reactions occur on the surface of nanostructure films. So the close-network structure of ZnO porous film should be considered to explain the enhanced sensing performance of the CNPAF sensor. It is worth noting that the gas-sensing response increased gradually with increase of specific surface area, which indicates that the large specific area will be well helpful for the gas detection.[27,45] In this paper, the CNPAF with close-network structure is primary explanation for enhanced sensing performance of the CNPAF sensor. On the one hand, it is well known that the reactions of the ZnO micro/nanoporous array sensors and the gas molecules takes place on the backbone of the micro/nanoporous array film. The primary cell surface areas of CNPAF and BLPAF were 0.494 and
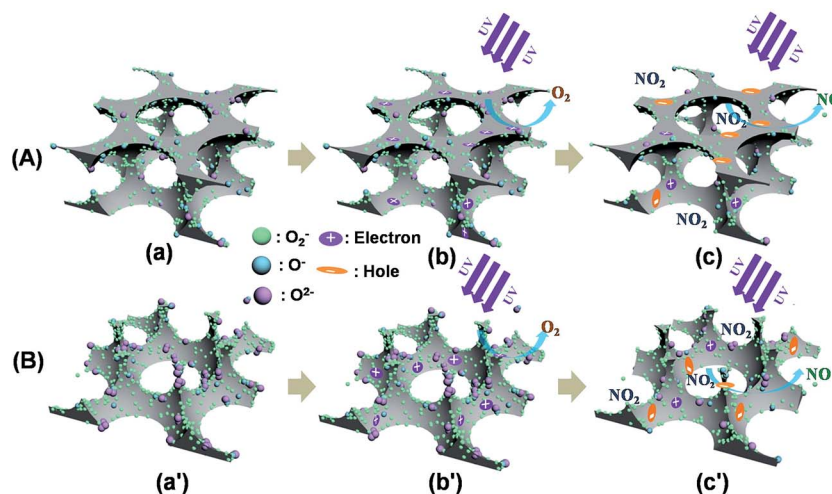

Fig. 7 Schematic of (A) ZnO close-network and (B) ZnO bowl-like porous array surface reactions under different conditions: (a) and (a') in the dark; (b) and (b') with UV light irradiation; (c) and (c') in NO_2 gas with UV light irradiation.
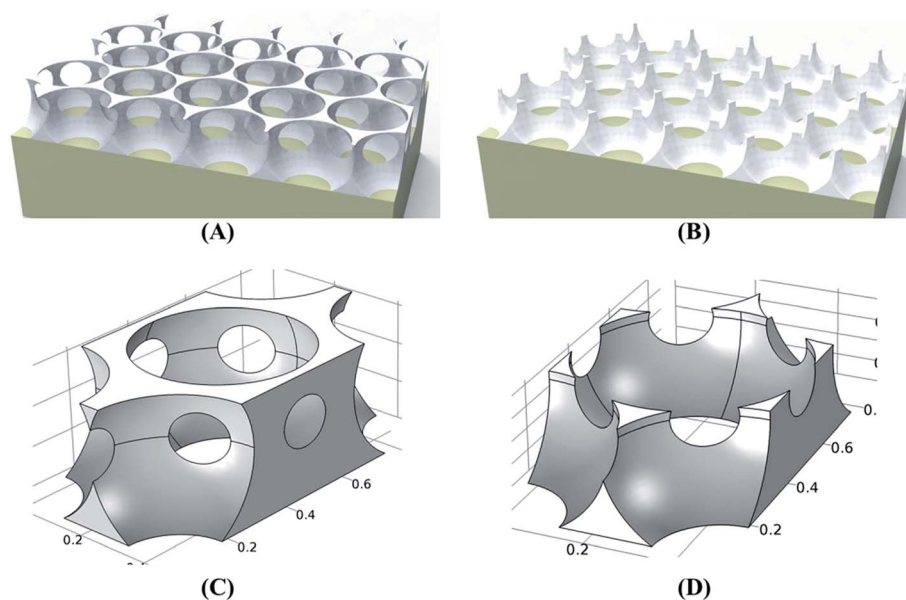
Fig. 8 Schematic view of ZnO micro/nanoporous porous film (A) CNPAF; (B) BLPAF. (C) and (D) Represent the unit cell of (A) and (B), respectively.

$0.303~\mu m^2$ by theoretical calculation (Fig. 8C and D), respectively. It is shown that the sensitive activation sites numbers of the CNPAF are more than that of the BLPAF in the reactions with the NO_2 gases. Correspondingly, the number of oxygen ions chemisorbing will be increased, resulting in the increase of the gas response for CNPAF sensor. On the other hand, one of the fundamental principles used in the analysis of response and recovery time is known as the hydrokinetic of microluidic flow. There is a small triangular hole at the interstitial position of the closely packed truncated hollow sphere, which may be produce "draught effect". It is a key factor that may promote the localized gas flowing, which thus lead to short response and recovery times of the sensor. This part of the experiment needs to be further confirmed.

Conclusion

In summary, the sensors based on CNPAF and BLPAF were prepared by transferring a solution-dipped self-organized colloidal template onto the flat ceramic electrode with different concentration of precursor solution and sequent heat treatment. Their sensing properties to NO_2 are studied in detail. Interestingly, compared with BLPAF-based sensors, the sensors of CNPAF exhibits shorter recovery and response times, higher sensitivity and better selectivity to NO_2 gas against other interfering gases. These enhanced sensing properties may be due to produce "draught effect", and provide more sensitive activation sites numbers of CNPAF to NO_2. This work clarified the morphology-correlated effect of ZnO micro/nanoporous arrays on their NO_2 sensing performances, and it would be helpful for the realization of NO_2 room temperature sensors.

Acknowledgements

References

1 C. Baratto, G. Sberveglieri, A. Onischuk, B. Caruso and S. D. Stasio, *Sens. Actuators, B*, 2004, **100**, 261.

2 L. Chen and S. C. Tsang, *Sens. Actuators, B*, 2003, **89**, 68.

3 J. S. Kima, J. W. Yoon, Y. J. Hong, Y. C. Kang, F. A. Hady, A. A. Wazzan and J. H. Lee, *Sens. Actuators, B*, 2016, **229**, 561.

4 Y. X. Li, B. Y. Zu, Y. N. Guo, K. Li, H. B. Zeng and X. C. Dou, *Small*, 2016, **12**, 1420.

5 S. H. Park, S. Y. An, Y. G. Mun and C. M. Lee, *Curr. Appl. Phys.*, 2014, **14**, 57.

6 Y. X. Qin, X. J. Zhang, Y. Liu and W. W. Xie, *J. Alloys Compd.*, 2016, **673**, 364.

7 T. Hyodo, K. Sasahara, Y. Shimizu and M. Egashira, *Sens. Actuators, B*, 2005, **106**, 580–590.

8 C. J. Chang, C. K. Liu, C. C. Chen, C. Y. Chen and E. H. Kuo, *Thin Solid Films*, 2011, **520**, 1546–1553.

9 T. Hamaguchi, N. Yabuki, M. Uno, S. Yamanaka, M. Egashira, Y. Shimizu and T. Hyodo, *Sens. Actuators, B*, 2006, **113**, 852–856.

10 C. J. Chang, C. Y. Liu, J. K. Chen and M. H. Hsu, *Ceram. Int.*, 2014, **40**, 10867–10875.

11 K. Dunst, D. Jurków and P. Jasiński, *Sens. Actuators, B*, 2016, **229**, 155.

12 V. Blechta, M. M. Karolin, V. V. Drogowska and M. Kalbá, *Sens. Actuators, B*, 2016, **226**, 299.

13 J. H. Yoon and J. S. Kim, *Solid State Ionics*, 2011, **192**, 668.

14 Y. L. Wang, X. B. Cui, Q. Y. Yang, J. Liu, Y. Gao, P. Sun and G. Y. Lu, *Sens. Actuators, B*, 2016, **225**, 544.

15 P. V. Adhyapak, S. P. Meshram, A. A. Pawar, D. P. Amalnerkar, U. P. Mulik and I. S. Mulla, *Ceram. Int.*, 2014, **40**, 12105.

16 T. Wagner, C. D. Kohl, C. Malagù, N. Donato, M. Latino, G. Neri and M. Tiemann, *Sens. Actuators, B*, 2013, **187**, 488.

17 E. Comini, G. Faglia and G. Sberveglieri, *Sens. Actuators, B*, 2001, **78**, 73.

18 S. J. Pearton, F. Ren, Y. L. Wang, B. H. Chu, K. H. Chen, C. Y. Chang, W. Lim, J. S. Lin and D. P. Norton, *Prog. Mater. Sci.*, 2010, **55**, 1.

19 S. Mishra, C. Ghanshyam, N. Ram, R. P. Bajpai and R. K. Bedi, *Sens. Actuators, B*, 2004, **97**, 387.

20 L. Peng, Q. D. Zhao, D. J. Wang, J. L. Zhai, P. Wang, S. Pang and T. F. Xie, *Sens. Actuators, B*, 2009, **136**, 80.

21 D. An, Y. Li, X. X. Lian, Y. L. Zou and G. Z. Deng, *Colloids Surf., A*, 2014, **447**, 81.

22 P. Afzali, Y. Abdi and E. Arzi, *Sens. Actuators, B*, 2014, **195**, 92.

23 S. G. Park, G. J. Sun, C. Y. Jin, H. W. Kim, S. M. Lee and C. M. Lee, *ACS Appl. Mater. Interfaces*, 2016, **8**, 2805.

24 L. N. Han, D. J. Wang, J. B. Cui, L. P. Chen, T. F. Jiang and Y. H. Lin, *J. Mater. Chem.*, 2012, **22**, 12915.

25 L. Luo, B. D. Sosnowchik and L. W. Lin, *Nanotechnology*, 2010, **21**, 495.

26 Y. X. Cai, X. W. Li, P. Sun, B. Wang, F. G. Liu, P. F. Cheng, S. S. Du and G. Y. Lu, *Mater. Lett.*, 2013, **112**, 36.

27 S. H. Park, H. S. Ko, S. M. Lee, H. W. Kim and C. M. Lee, *Thin Solid Films*, 2014, **570**, 298.

28 K. Kourosh, V. Aravind, H. Moon, H. Zheng, B. Michael and M. S. Strano, *Chem. Mater.*, 2010, **19**, 5660.

29 J. B. Cui, L. Q. Shi, T. F. Xie, D. J. Wang and Y. H. Lin, *Sens. Actuators, B*, 2016, **227**, 220.

30 J. L. Zhai, L. L. Wang, D. J. Wang, Y. H. Lin, D. Q. He and T. F. Xie, *Sens. Actuators, B*, 2012, **161**, 292.

31 J. Gong, Y. H. Li, X. S. Chai, Z. S. Hu and Y. L. Deng, *J. Phys. Chem. C*, 2010, **114**, 1293.

32 G. T. Duan, W. P. Cai, Y. Li, B. Q. Cao and Y. Y. Luo, *J. Phys. Chem. B*, 2006, **14**, 7184.

33 Y. X. Li, N. Chen, D. Y. Deng, X. X. Xing, X. C. Xiao and Y. D. Wang, *Sens. Actuators, B*, 2017, **238**, 264.

34 H. Y. Du, J. Wang, P. Yu, N. S. Yu, Y. H. Sun and J. L. Tian, *J. Nanopart. Res.*, 2014, **16**, 2216.

35 G. T. Duan, W. P. Cai, Y. Y. Luo and F. F. Sun, *Adv. Funct. Mater.*, 2007, **17**, 644.

36 Z. K. Xu, G. T. Duan, Y. Li, G. Q. Liu, H. W. Zhang, Z. F. Dai and W. P. Cai, *Chem.–Eur. J.*, 2014, **20**, 1.

37 H. W. Zhang, G. T. Duan, G. Q. Liu, Y. Li, X. X. Xu, Z. F. Dai and J. J. Wang, *Nanoscale*, 2013, **5**, 2460.

38 L. C. Jia, W. P. Cai and H. Q. Wang, *J. Mater. Chem.*, 2009, **19**, 7301.

39 S. W. Fan, A. K. Srivastava and V. P. Dravid, *Appl. Phys. Lett.*, 2009, **95**, 14210.

40 N. Yamazoe, G. Sakai and K. Shimanoe, *Catal. Surv. Asia*, 2003, **7**, 63.

41 T. Lei, S. P. Zhang, D. Li, W. Zhang, S. Huang and C. S. Xie, *Sens. Actuators, B*, 2014, **199**, 15.

42 Y. Mun, S. Park, S. An, C. Lee and H. W. Kim, *Ceram. Int.*, 2013, **39**, 8615.

43 S. L. Bai, L. Y. Chen, D. Q. Li, W. S. Yang, P. C. Yang, Z. Y. Liu, A. Chen and C. L. Chung, *Sens. Actuators, B*, 2010, **146**, 129–137.

44 S. Öztürk, N. Kılınç, N. Taşaltin and Z. Z. Öztürk, *Thin Solid Films*, 2011, **520**, 932–938.

45 J. B. Cui, L. Q. Shi, T. F. Xie, D. J. Wang and Y. Lin, *Sens. Actuators, B*, 2015, **227**, 220.